ACS BIO & MED CHEM Au
AN OPEN ACCESS JOURNAL OF THE AMERICAN CHEMICAL SOCIETY

Editors' Choice
Open Access

pubs.acs.org/biomedchemau
Article

An Investigation of Nirmatrelvir (Paxlovid) Resistance in SARS-CoV-2 M^{pro}

Rasha M. Yaghi, Dennis C. Wylie, Collin L. Andrews, Olivia H. Dickert, Anjana Ram, and Brent L. Iverson*

Cite This: *ACS Bio Med Chem Au* 2024, 4, 280−290
Read Online

ACCESS | Metrics & More | Article Recommendations | Supporting Information

ABSTRACT: The high throughput YESS 2.0 platform was used to screen a large library of SARS-CoV-2 M^{pro} variants in the presence of nirmatrelvir. Of the 100 individual most prevalent mutations identified in the screen and reported here, the most common were E166V, L27V, N142S, A173V, and Y154N, along with their various combinations. *In vitro* analysis revealed that resistance to nirmatrelvir for these individual mutations, as well as all of the combinations we analyzed, was accompanied by decreased catalytic activity with the native substrate. Importantly, the mutations we identified have not appeared as significantly enriched in SARS-CoV-2 M^{pro} sequences isolated from COVID-19 patients following the introduction of nirmatrelvir. We also analyzed three of the most common SARS-CoV-2 M^{pro} mutations that have been seen in patients recently, and only a measured increase in nirmatrelvir resistance was seen when the more recently appearing A285V is added to both P132H and K90R. Taken together, our results predict that resistance to nirmatrelvir will be slower to develop than expected based on experience with other viral protease inhibitors, perhaps due in part to the close structural correspondence between nirmatrelvir and SARS-CoV-2 M^{pro}'s preferred substrates.

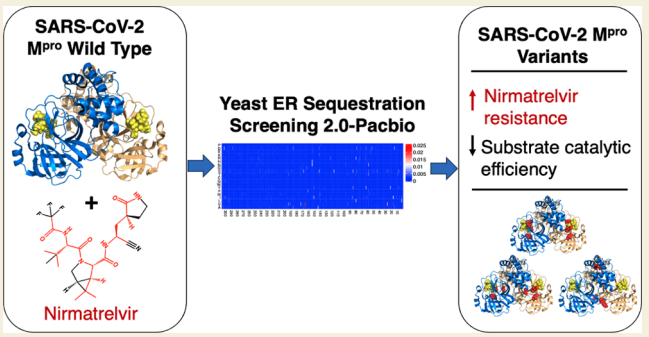

KEYWORDS: *protease, YESS, COVID-19, Paxlovid, nirmatrelvir resistance*

INTRODUCTION

The main protease in SARS-CoV-2, M^{pro} (EC 3.4.22.69), is a Cys protease from the coronavirus disease 2019 (COVID-19) that is also known as the C30 endopeptidase or 3-chymotrypsin-like Cys protease ($3CL^{pro}$).[1] A programmed −1 ribosomal frameshift in SARS-CoV-2 produces two overlapping reading frames, ORF1a and ORF1b, leading to two polyproteins: pp1a, coding for nonstructural proteins 1−11 (nsp1−nsp11) and pp1b, coding for nsp1−nsp10, nsp12−nsp16.[2,3] The polyproteins are cleaved by two proteases during the viral maturation process, the papain-like protease (PL^{pro})[4] and SARS-CoV-2 M^{pro}.[5] Pp1a is cleaved by SARS-CoV-2 M^{pro} after nsp4−nsp10 while pp1b is cleaved by SARS-CoV-2 M^{pro} after nsp4−nsp10 and after nsp12−nsp15, with a total of 11 unique sites in pp1a/pp1b. We have recently completed a comprehensive substrate specificity profile of SARS-CoV-2 M^{pro}, revealing a modest preference for Val at both P4 and P3, a stronger preference for Leu at P2, an absolute preference for Gln at P1, and then a preference for small side chains (Gly, Ala, Ser, Cys) in the P1′ position. No preferences were found for the P2′−P4′ positions other than a strong preference against Pro at P2′.[6]

Paxlovid

Nirmatrelvir (also known as PF-07321332), in combination with the potent CYP3A4 inhibitor ritonavir to slow metabolism, is marketed as Paxlovid by Pfizer and presently serves as an effective front-line treatment for COVID-19 in several countries.[7] Nirmatrelvir is a reversible covalent inhibitor that targets M^{pro} with a nitrile "warhead". Nirmatrelvir was developed as a second generation M^{pro} inhibitor specifically to treat COVID-19 infections based on first generation M^{pro} inhibitors[8,9] that were originally developed to target M^{pro} of SARS-CoV as well as other members of the *Coronaviridae* family of viruses. Importantly, nirmatrelvir is a peptidomimetic that resembles the P1−P3 side chains of native M^{pro} substrates. Particularly noteworthy is the pyrrolidone group in nirmatrelvir that serves as a conformationally restricted mimic of the preferred P1 Gln substrate residue.[6,8−10] There are groups on nirmatrelvir that target the P2 and P3 sites as well, resembling the Leu and Val side chains, respectively, preferred as those sites of the substrate. Because there are no known human Cys proteases with a requirement for Gln at P1, the combination of the nitrile warhead and Gln mimic at P1 is thought to ensure

Received: June 20, 2024
Revised: August 14, 2024
Accepted: August 15, 2024
Published: October 8, 2024

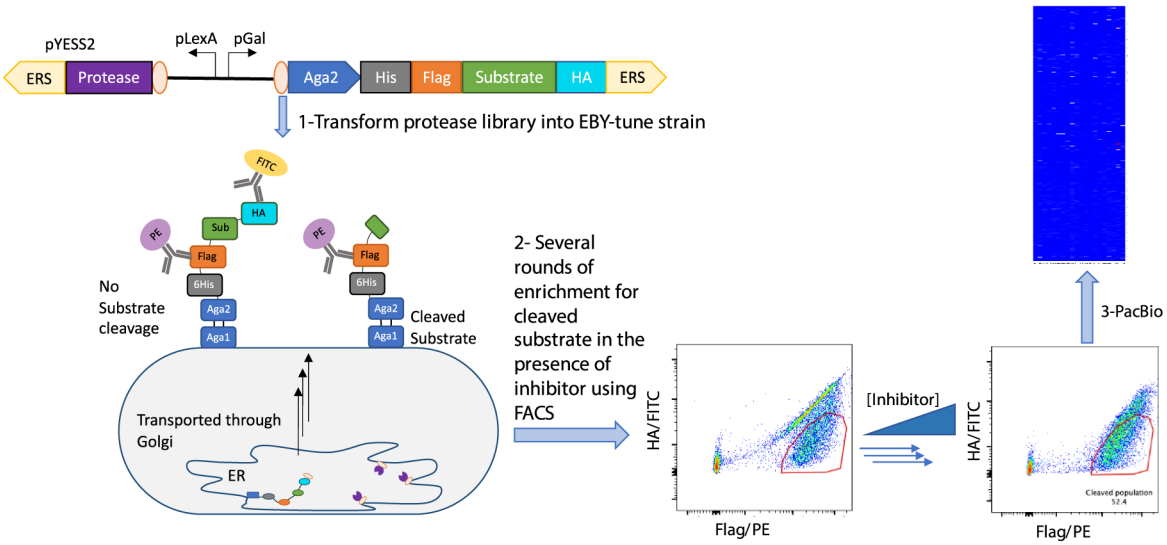

Figure 1. Yeast ER sequestration screening (YESS2.0)-PacBio Resistance mutation screen overview. pYESS2 plasmid containing the protease substrate of interest is transformed along with the protease library into yeast. The resistance mutation screen is carried out by sorting for the loss of the HA/FITC signal in the presence of inhibitor. After several rounds of sorting with increased stringency, the DNA is extracted and sent for PacBio sequencing, and data is analyzed to obtain heatmaps.

effective viral targeting in humans. Paxlovid was given an emergency use authorization by the FDA in December of 2021.

Based on experience with protease inhibitors such as those used to treat HIV,[11,12] an obvious concern with Paxlovid is the possible emergence of drug resistance mutations that could render it considerably less effective.[13] A pattern seen with AIDS protease inhibitors is that a primary initial mutation arises that confers resistance, but that initial mutation often compromises viral viability.[11] Additional secondary mutations then accumulate that preserve the drug resistance but improve viral viability.[11] A number of studies using a variety of platforms, including passage through mammalian cells and also yeast,[14,15] have recently been published exploring possible Paxlovid resistance mutations,[14−35] including an E166V[14,15,18,20−22,24,26,30,33] mutation that confers drug resistance but also compromises viral viability. Several other mutations have been observed, including T21I, L50F, S144A, E166A, L167F, A173V, and T304I,[20,23,24,29−35] and the number of publications discussing possible Paxlovid resistance mutations continues to increase. When analyzed, these mutations, alone and in combinations, have generally been reported to provide resistance to nirmatrelvir at the expense of enzymatic activity with native peptide substrates.

As of April 2024, three SARS-CoV-2 M^{pro} mutations (relative to the very first clinical isolate) are commonly appearing together in genome isolates from COVID-19 patients reported in the GISAID database.[36] P132H appeared in June 2020 and was soon found commonly in clinical isolates. The combination of P132H and K90R appeared in November 2020 and became common throughout 2021. The combination of P132H, K90R, and A285 V is currently common, having first appeared in May 2022 (following the approval of Paxlovid for emergency use), although A285V first appeared in 2020.

Yeast Endoplasmic Reticulum Sequestration Screening 2.0 (YESS 2.0)

The YESS 2.0 platform places both the protease and a substrate in the yeast endoplasmic reticulum where they can interact, then the substrate fusion is displayed on the yeast outer surface via the well-known Aga1−Aga2 interaction (Figure 1).[37] Different antibody binding epitopes flanking either side of the putative protease substrate sequence are used to quantify the substrate cleavage using fluorescence activated cell sorting (FACS) in the presence of the appropriate labeled antibodies. Protease and substrate expression is independently controlled using β-estradiol and galactose, respectively, allowing for precise optimization and reproducibility of reaction conditions.[37] Note that by sequestering the protease of interest, in this case SARS-CoV-2 M^{pro}, in the endoplasmic reticulum, toxicity is eliminated, unlike other systems in which the protease is expressed in the yeast cytoplasm.[14] For this reason, our results using YESS 2.0 are free of artifacts derived from host toxicity concerns.

The YESS 2.0 system can be used to explore drug resistance efficiently by sorting a large library (>10^8) of protease variants for activity in the presence of an inhibitor followed by PacBio sequencing[38] of the population of active and therefore resistant clones (Figure 1).[39] Analyzing the population of active variants can identify different protease mutations that confer resistance. Using PacBio sequencing makes possible the identification of mutations that are functionally coupled with each other (i.e., epistatic) in a given variant, even when they are an extended distance away in primary sequence. The important point to emphasize is that YESS 2.0 is a very high throughput methodology, exploring large segments of sequence space capable of delivering well over a hundred individual selected mutations.

Herein is reported the results of using YESS 2.0 with SARS-CoV-2 M^{pro} to carry out a comprehensive analysis of nirmatrelvir resistance. In particular, screening of a variant library of SARS-CoV-2 M^{pro}, generated by error-prone PCR across the entire

https://doi.org/10.1021/acsbiomedchemau.4c00045
ACS Bio Med Chem Au 2024, 4, 280−290

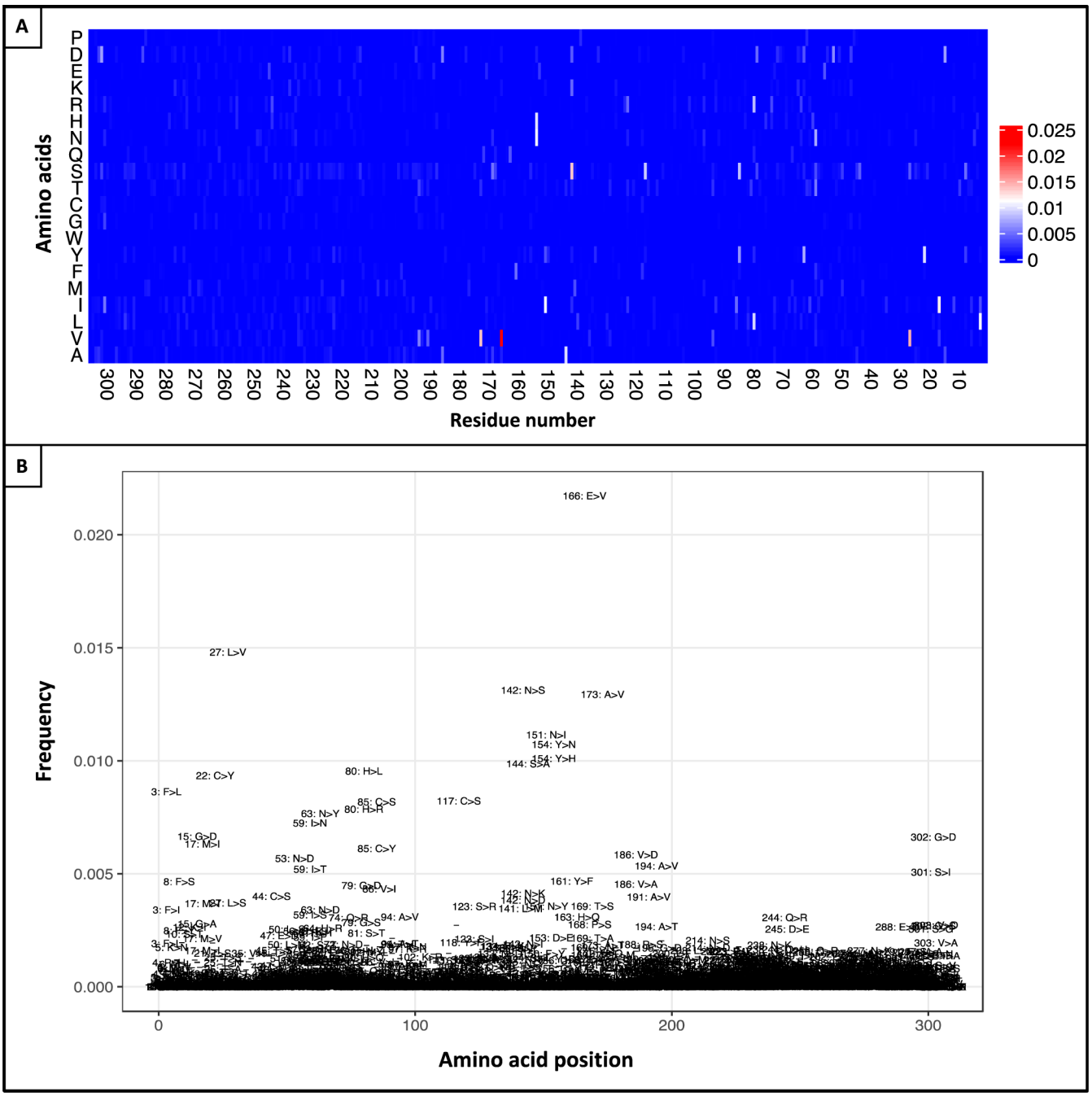

Figure 2. SARS-CoV-2 M^{pro} resistance mutation identified by screening in the presence of nirmatrelvir. (A) SARS-CoV-2 M^{pro} enriched mutations heatmap. (B) SARS-CoV-2 M^{pro} enriched mutations frequency plot.

gene, in the presence of nirmatrelvir produced a large collection of resistant variants involving mutations such as E166V, L27V, N142S, A173V, and Y154N as well as some specific combinations. Several of the most prevalent individual mutations and the most common combinations were characterized *in vitro*, revealing that strong resistance to nirmatrelvir comes at the expense of decreased catalytic activity with the original substrates, which would be expected to compromise viral replication. We also analyzed (alone and in combination) the three SARS-CoV-2 M^{pro} mutations that commonly appear in current patients, P132H, K90R, and A285V. P132H appears to compromise the overall catalytic activity of SARS-CoV-2 M^{pro}, while K90R appears to restore it, perhaps above even the original levels. A285V provides some modest resistance to nirmatrelvir alone or in combination, but it does so at the expense of catalytic efficiency by virtue of a significantly increased K_M value. Taken together, our results predict that resistance to nirmatrelvir will be relatively slow to develop, likely due in part to the close similarity of the nirmatrelvir structure to that of the SARS-CoV-2 M^{pro} substrates.[40]

RESULTS

Nirmatrelvir Resistance Mutation Screen of SARS-CoV-2 M^{pro}

Previously, we found that SARS-CoV-2 M^{pro} without an attached ERS sequence showed strong substrate cleavage in

https://doi.org/10.1021/acsbiomedchemau.4c00045
ACS Bio Med Chem Au 2024, 4, 280−290

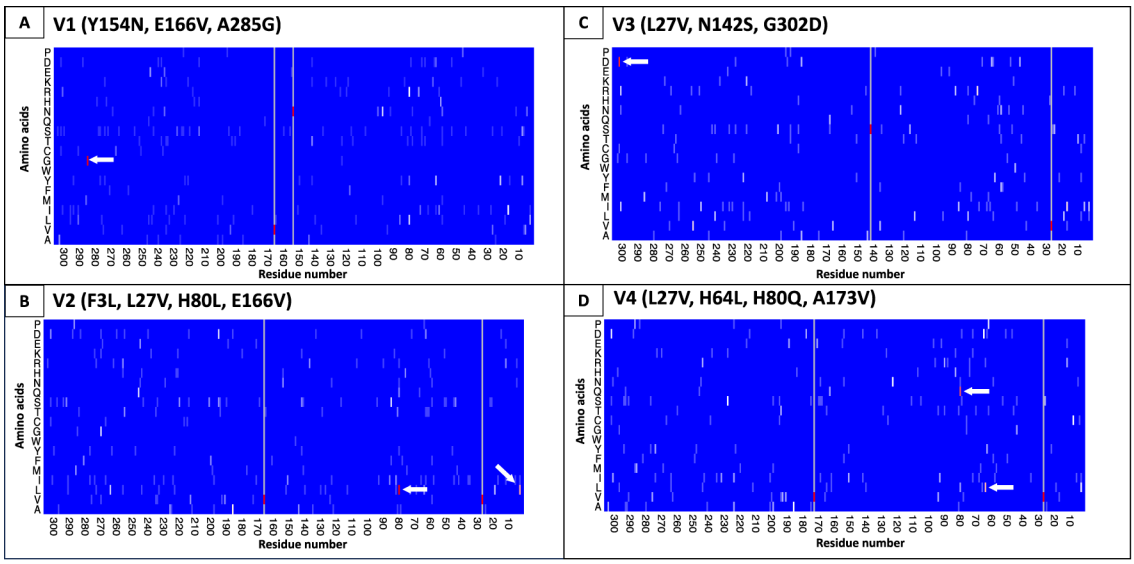

Figure 3. Nirmatrelvir inhibition of combination mutation variants of SARS-CoV-2 M^{pro} heatmap. (A) Heatmap of the sequence population that contains both E166V and Y154N shows enrichment for A285G. (B) Heatmap of the sequence population that contains both L27V and E166V shows enrichment for F3L and H80L. (C) Heatmap of the sequence population that contains both L27V and N142S shows enrichment for G302D. (D) Heatmap of the sequence population that contains both L27V and A173V shows enrichment for H64L and H80Q. White arrows indicate highly enriched residues.

YESS 2.0. Using this construct, we were able to develop a high-resolution profile of SARS-CoV-2 M^{pro} substrate specificity.[6] In order to identify resistance mutations, yeast containing the WT SARS-CoV-2 M^{pro} and the AVLQ↓SGFR substrate sequence was analyzed by FACS after incubation with increasing concentrations of nirmatrelvir, and a corresponding decrease in substrate cleavage was observed (Figure S1), verifying penetration of the drug into the yeast ER. A SARS-CoV-2 M^{pro} library containing ~2×10^8 variants was constructed by using error-prone PCR and cloned into the YESS 2.0 system. The library was screened against increasing concentrations of nirmatrelvir over 7 rounds of sorting, the point at which the population was no longer shifting toward greater substrate cleavage (see Figure S2). Increasing the nirmatrelvir concentration over 7 rounds of sorting was intended to increase stringency, while making sure to include the entire population of even rare resistant clones in the early rounds.

DNA from the final sorted round (round 7) population of yeast was isolated and sequenced using PacBio so that the different mutations across each individual SARS-CoV-2 M^{pro} gene could be correlated with each other, and the different isolated genes compared across the population. A heatmap of the enriched residue mutations is seen in Figure 2A, and the most frequent mutations are shown as a frequency versus position plot in Figure 2B. By far, the most common mutation identified in the screen was E166V, followed by L27V, N142S, and A173V to round out the top four. The other most common mutations listed in the descending order of frequency are N151I, Y154N, Y154H, S144A, H80I, C22Y, F3L, C85S, C117S, H80R, N63Y, I59N, G15D, M17I, G302D, C85Y, N53D, V186D, A194V, and I59T. The 10 most common mutations (E116V, L27V, N142S, A173V, N151I, Y154N, H80L, S301I, C117S, and N53D) were examined individually by FACS for inhibition, and all 10 displayed more activity in the presence of nirmatrelvir compared to the original SARS-CoV-2 M^{pro} (Figure S3). Table S1 lists the nucleotide changes responsible for the 100 most common mutations identified in our screen, with observed counts ranging from 34130 counts for the most common mutation E166V to 2547 counts for the 100th most common mutation Q256R. Of these 100 most common mutations, it is noteworthy that the vast majority are present in the GISAID database at very low levels. Those few mutations present in the largest numbers of sequences, M17I, T169S, A94V, T93I, F223L, and M17V, first appeared before Paxlovid was in widespread use and do not appear to be increasing in prevalence now that Paxlovid has become a frontline treatment.

Taking advantage of the PacBio sequencing that provides the sequence of entire variant enzyme genes, all of the sequences containing some of the most common mutations were examined to identify any mutations that are overrepresented in those populations, suggesting possible synergistic function (see Figures 3 and S4). In particular, when examining all of the sequences that contain the most common mutation E166V, the mutation Y154N is also found to be enriched. When looking at only those sequences containing both E166V and Y154N, the mutation A285G is also found to be significantly enriched (E166V, Y154N, and A285G are called V1, Figures 3A and S4A). When examining all of the sequences that contain the second most common mutation, L27V, both E166V and L142S are also found to be highly enriched. When looking only at the sequences that contain both L27V and E166V, the mutations F3L and H80L were also found to be enriched (L27V, E166V, F3L, and H80L are called V2, Figures 3B and S4B). Similarly, when examining only those sequences that contain both L27V and N142S, the mutation G302D was also found to be enriched (L27V, N142S, and G302D are called V3, Figures 3C and S4C). Finally, examining only those sequences containing A173V, the mutations L27V, H64L, and H80Q were found to be also enriched (A173V, H64L, and H80Q are called V4, Figures 3D and S4D).

Analysis of Resistant Clones

A total of 11 different single mutation variants and the 4 combination mutation variants V1−V4 were cloned, expressed, purified, and evaluated using a FRET-based *in vitro* assay with an

https://doi.org/10.1021/acsbiomedchemau.4c00045
ACS Bio Med Chem Au 2024, 4, 280−290

Table 1. Kinetic Parameters of SARS-CoV-2 M^{pro}[a]

variant	mutations	apparent K_i (μM)	K_M (μM)	k_{cat} (min^{-1})	k_{cat}/K_M (μM^{-1}min^{-1})	$(K_i/K_M) * k_{cat}$ (min^{-1})	GISAID counts
WT	-	0.002 ± 0.0004	16 ± 1.6	200 ± 5.7	12.5	0.02	-
VI	Y154N_E166V_A285G	63 ± 5.3	200 ± 30	74 ± 8	0.4	22.7	-
	Y154N_E166V	43 ± 3.4	160 ± 38	33 ± 5.3	0.2	8.8	-
	Y154N	0.016 ± 0 003	21 ± 3.4	240 ± 13	11.3	0.2	3
	E166V	73 ± 5	270 ± 67	35 ± 6.9	0.1	9.6	56
	A285G	0.009 ± 0002	65 ± 13	27 ± 2.8	0.4	0.004	37
V2	F3L_L27V_H80L_E166V	18 ± 3.6	12 ± 1	15 ± 0.4	1.3	22.8	-
	L27V_El66V	20 ± 9.4	88 ± 19	10 ± 1 3	0.1	2.2	-
	F3L	0.003 ± 0.001	5.3 ± 1.2	59 ± 2.5	11.2	0.03	82
	L27V	0.01 ± 0.004	3.7 ± 0.2	10.0 ± 0.12	2.7	0.02	25
	H80L.	0 002 ± 0 0008	6 ± 1.2	130 ± 5.5	21.7	0.04	6
	E166V	73 ± 5	270 ± 67	35 ± 6.9	0.1	9.6	-
V3	L27V_N142S_G302D	0.019 ± 0.005	3.3 ± 0.4	17.0 ± 0.3	5.1	0.1	-
	L27V	0.01 ± 0.004	3.7 ± 0.2	10.0 ± 0 12	4.5	0.03	25
	N142S	0.004 ± 0.001	27 ± 5.7	230 ± 18	8.7	0.03	255
	G302D	0.006 ±0.001	17 ± 4.7	36 ± 3	2.1	0.01	3
V4	A173V_L27V_H64L_H80Q	0.42 ± 0 03	16 ± 1.7	19.3 ± 0.6	1.2	0.45	-
	L27V	0.01 ± 0 004	3.7 ± 0.2	10.0 ± 0.12	4.5	0.03	25
	H64L	0.009 ± 0.001	19 ± 5.2	220 ± 19	11.6	0.1	10
	H80Q	0.005 ± 0.002	23 ± 4.7	140 ± 9.9	6.3	0.03	33
	A173V	0.007 ± 0.002	20 ± 2.1	142 ± 4.7	7.2	0.05	296
GISAID mutations[b]	K90R	0.001 ± 0.0001	28 ± 4.9	130 ± 8.7	5.0	0.005	221707
	P132H	0.002 ± 0.0007	17 ± 1.3	65 ± 1.5	3.9	0.01	9110789
	A285V	0.06 ± 0 006	73 ± 15	54 ± 5.8	0.7	0.04	8320
	K90R-P132H	0.003 ± 0.0006	25 ± 2.3	290 ± 9	11.6	0.03	58449
	K90R-P132H-A285V	0.02 ± 0.003	87 ± 9.3	170 ± 10.7	2.0	0.04	2214

[a]All kinetic analyses were carried out in triplicate. [b]Mutations identified in the GISAID database as of July, 2024.[42]

(Abz)AVLQ↓SGFR(K-DNP) substrate (Table 1). The 11 single mutation variants chosen represent all of the individual mutations seen in the combination variants analyzed and include the most abundant mutations seen in the population of mutations selected in the presence of nirmatrelvir. In addition, 2 double mutation variants were analyzed (Y154N, E166V and L27V, E166V) because these combinations were so prevalent in the selected variant pool. Apparent K_i values are listed in Table 1 along with the catalytic parameters for the (Abz)AVLQ↓SGFR(K-DNP) substrate. The K_i values listed in Table 1 are referred to as "apparent K_i" values because of the reversible, covalent nature of nirmatrelvir binding that introduces bond-making and bond-breaking rate constants that must be considered along with the individual noncovalent on-rates and off-rates (only the latter two would define a proper K_i value).[41]

As seen in Table 1, E166V was the most effective resistance mutation identified in our study and was over 35000-fold more resistant to nirmatrelvir compared to the original SARS-CoV-2 M^{pro}. Importantly, however, for E166V, the reaction with the AVLQ↓SGFR itself was also around 150-fold compromised (comparing k_{cat}/K_M values) compared to the original SARS-CoV-2 M^{pro}. Relative to E166V, the other individual mutations selected most often in our screen showed significantly more modest levels of resistance, exhibiting an apparent K_i that is only between 2- and 4-fold higher than the original SARS-CoV-2 M^{pro}. These changes displayed a range of consequences for the reaction with the substrate. For example, of the single amino acid variants we identified, H80L was noteworthy in that due to a significantly lower K_M value (6 mM), it displayed a catalytic efficiency (k_{cat}/K_M) value with AVLQ↓SGFR that was even higher than the original SARS-CoV-2 M^{pro}. The H64L and Y154N variants displayed both k_{cat} and K_M values (and therefore a catalytic efficiency) similar to those of the original SARS-CoV-2 M^{pro}. On the other hand, although both the F3L and N142S variants also exhibited catalytic efficiency (k_{cat}/K_M) values about the same as the original SARS-CoV-2 M^{pro}, both their K_M and k_{cat} values were somewhat lower. The H80Q and A173V variants had a somewhat lower k_{cat} value and similar K_M value compared to those of the original SARS-CoV-2 M^{pro}. The L27V variant displayed a lower K_M value along with a very compromised k_{cat} value compared to the original SARS-CoV-2 M^{pro}, while G302D and A285G displayed k_{cat}/K_M values that were even lower, also the result of compromised k_{cat} values. Both double mutation variants that contain E166V (Y154N, E166V, and L27V, E166V) were a little less resistant than E166V alone, but both also displayed a lower K_M value with the AVLQ↓SGFR substrate.

The four combination variants V1−V4 were also analyzed using the FRET-based peptide cleavage assay. Note that a FACS analysis using the YESS 2.0 constructs indicated that V1−V4 were all qualitatively more resistant to nirmatrelvir compared to the original SARS-CoV-2 M^{pro} (Figures S5 and S6). From the *in vitro* FRET peptide cleavage data (Table 1), the combination mutations that displayed the most resistance to nirmatrelvir inhibition compared to the original SARS-CoV-2 M^{pro}, termed V1 and V2, both contained the highly resistant E166V mutation. While V1 was about as resistant to nirmatrelvir inhibition as E166V alone, V1 was around 3-fold more efficient as k_{cat}/K_M when reacting with the AVLQ↓SGFR substrate compared to E166V. Compared to E166V alone, V2 was about 4-fold less resistant to nirmatrelvir inhibition, but it was 9-fold more efficient as k_{cat}/K_M reacting with the AVLQ↓SGFR substrate.

https://doi.org/10.1021/acsbiomedchemau.4c00045
ACS Bio Med Chem Au 2024, 4, 280−290

Even so, V2 is still more than 15-fold compromised reacting with the AVLQ↓SGFR substrate compared to the original SARS-CoV-2 M^{pro}. The V3 variant displayed an apparent K_i value that was significantly lesser than that of the combination variants that contained E166V (V1 and V2). Nevertheless, V3 is more resistant than any of the individual mutations it contains and is still 5-fold more resistant to nirmatrelvir compared to the original SARS-CoV-2 M^{pro}. Even though the V3 resistance to nirmatrelvir is modest, it still displayed a roughly 4-fold compromised catalytic efficiency with the AVLQ↓SGFR substrate. Like V3, the V4 combination was more resistant to nirmatrelvir than either the original SARS-CoV-2 M^{pro} or any of its four mutations measured individually. However, V4 is also significantly less efficient at catalyzing the cleavage of the AVLQ↓SGFR substrate compared to any of its mutations measured individually or the original SARS-CoV-2 M^{pro}.

All of the individual mutations and mutation combinations listed in Table 1 were checked for their presence in the GISAID database,[36] and the number of occurrences is listed in the last column of Table 1. The GISAID database, with over 16.8 million sequences deposited to date, compiles SARS-CoV-2 virus sequences reported since the beginning of the COVID-19 pandemic. None of the mutation combinations (V1−V4) were found in any sequence deposited in GISAID. The A173V and N142S mutations have both been reported about 250 times. The F3L mutation has been reported 82 times, and all of the other mutations we identified are present in fewer than 50 deposited sequences.

Analysis of Common Mutations Identified in the GISAID Database[36]

The three SARS-CoV-2 M^{pro} mutations commonly seen in current COVID-19 patients, P132H, K90R, and A285V, were characterized alone and in combination using the AVLQ↓SGFR substrate in a FRET assay in the presence and absence of nirmatrelvir as well as a FACS screen (Table 1, Figure S7). The P132H variant demonstrated no increased resistance to nirmatrelvir but did display a more than 3-fold lower catalytic efficiency with the substrate, largely due to a decreased k_{cat} value. The K90R variant was slightly more sensitive to nirmatrelvir compared to either the original SARS-CoV-2 M^{pro} or the P132H variant, yet K90R was still about 2-fold less efficient reacting with the substrate. Interestingly, the P132H, K90R double variant recovered the original SARS-CoV-2 M^{pro} level of catalytic efficiency with the AVLQ↓SGFR substrate, displaying similarly higher overall K_M and k_{cat} values. Nevertheless, the P132H and K90R variants were as sensitive to nirmatrelvir as the original SARS-CoV-2 M^{pro}. The variant with the A285V mutation alone was over 10-fold more resistant to nirmatrelvir compared to the original SARS-CoV-2 M^{pro} but was about 10-fold less efficient as a catalyst with the AVLQ↓SGFR substrate. The triple mutation variant, P132H, K90R, and A285V, the variant that is currently seen commonly among clinical COVID-19 isolates, displayed a greater than 20-fold decrease in sensitivity to nirmatrelvir but is still about 6-fold compromised in catalytic activity with the AVLQ↓SGFR substrate when compared to the original SARS-CoV-2 M^{pro}.

DISCUSSION

As Paxlovid continues to be used as a frontline treatment for COVID-19, concern is naturally increasing about the emergence of SARS-CoV-2 M^{pro} resistance mutations that might inhibit nirmatrelvir binding while retaining polyprotein cleavage activity[14,16−35] and therefore viral viability. When our yeast containing SARS-CoV-2 M^{pro} and the AVLQ↓SGFR substrate in YESS 2.0 were incubated with nirmatrelvir, substrate cleavage was inhibited, indicating that nirmatrelvir successfully crosses into the yeast ER. Following error-prone mutagenesis of the entire SARS-CoV-2 M^{pro} gene and multiple rounds of increasingly stringent FACS sorting, hundreds of mutations were enriched as presented in Figure 2. In theory, selected mutations could inhibit nirmatrelvir binding, enhance overall catalytic efficiency with the AVLQ↓SGFR substrate, or do both simultaneously. By using PacBio sequencing to allow for accurate identification of multiple mutations within the same variant, we examined the possibility of synergistic or even epistatic mutation patterns.

The most prevalent mutation to appear in our final sorted library was E166V, a mutation that has appeared in several other nirmatrelvir resistance studies[14,15,18,20−22,24,26,30,33] using SARS-CoV-2 M^{pro}. In our peptide cleavage assay, E166V was found to have a nirmatrelvir apparent K_i of 73 μM. On the other hand, the E166V variant was found to be about 150-fold less efficient (k_{cat}/K_M) at catalyzing the cleavage of the AVLQ↓SGFR substrate compared to the original SARS-CoV-2 M^{pro}, raising questions about the viability of this mutation to support viral replication. The fact that E166V simultaneously disrupts nirmatrelvir binding as well as substrate cleavage is not surprising, because in the SARS-CoV-2 M^{pro} active site, Glu 166 makes key hydrogen bonds to the pyrrolidone group of nirmatrelvir[10] as well as important hydrogen bonds with the P1 Gln side chain of the substrate.[43,44] This is not a coincidence as the nirmatrelvir pyrrolidone can be viewed as a structural mimic of the P1 Gln side chain[7−9] (see Figure 4). It is interesting to note that the Glu 166 side chain also interacts with the Ser 1 of the other subunit of the active SARS-CoV-2 M^{pro} dimer.[45] Losing this interchain interaction could thus further disrupt enzymatic activity with the substrate. The E166V mutation has only appeared in 56 entries of the GISAID COVID-19 genome sequence database to date, indicating that it is not yet an emerging resistance mutation, no doubt due to its compromised viral viability. We note that E166Q has appeared over 4500 times; however, it first appeared in 2020 and previous studies reported similar catalytic activity compared to wild-type SARS-CoV-2 M^{pro} and no significant resistance to nirmatrelvir.[24]

Interestingly, beyond E166V, each of the other three most common mutations isolated in our screen either contacts the substrate/nirmatrelvir directly (L27V, N142S) or is in the active site second shell (A173V) (see the red side chains in Figure 5A). Like E166V, the influence of these three mutations on inhibitor binding and substrate reactivity is therefore likely to be due to direct interactions. The somewhat less common, but still relatively prevalent, mutations that we identified and studied (F3L, H64L, H80L, Y154N, G302D, violet side chains in Figure 5A) are all well outside of the active site. These latter mutations likely influence nirmatrelvir binding and substrate reactivity through interactions that are more indirect in nature.

In order to investigate possible synergy or epistasis between multiple mutations in the same variant, our sorted population was filtered to identify the most highly enriched mutation combinations. For example, in the E166V-containing population of selected variant sequences, Y154N is the most significantly coenriched. We therefore filtered the selected population to obtain only those sequences with both E166V and Y154N, leading to the strong coenrichment of A285G (see Figure 3A). This E166V, Y154N, A285G triple mutation variant, called V1

https://doi.org/10.1021/acsbiomedchemau.4c00045
ACS Bio Med Chem Au 2024, 4, 280−290

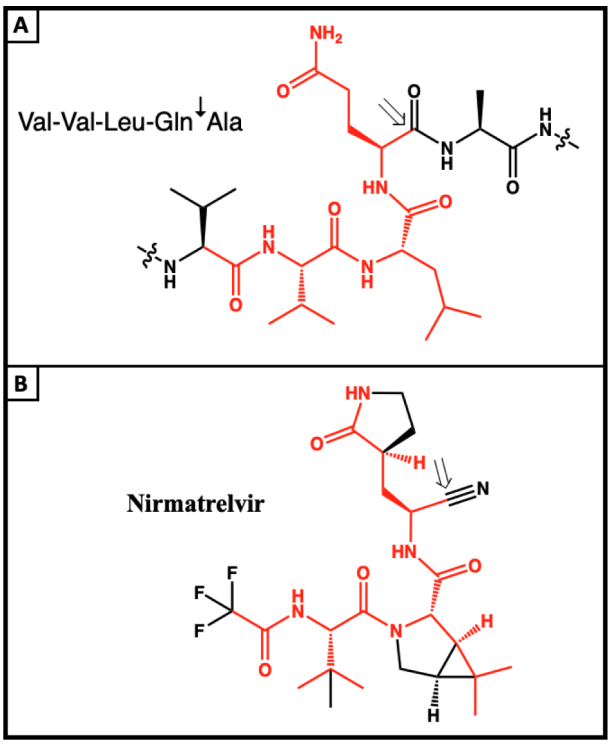

Figure 4. Comparison of the SARS-CoV-2 M^{pro} preferred substrate with the structure of nirmatrelvir. (A) A preferred substrate for SARS-CoV-2 M^{pro} identified from high-resolution substrate profiling[6] with atoms homologous to the nirmatrelvir structure in red. (B) The structure of nirmatrelvir with homologous atoms from the preferred substrate is traced in red. The location of the nucleophilic attack by the enzyme is indicated by an arrow in both structures.

(see Figure S4A), was expressed and analyzed *in vitro* along with the E166V, Y154N, and A285G single mutation variants individually as well as the E166V, Y154N double mutation variant. V1 mostly retained strong resistance to nirmatrelvir binding of the E166V mutation. In addition, AVLQ↓SGFR substrate cleavage activity of V1 was better than the E166V variant, but only by 3-fold, apparently enough to show up as an enriched combination in our sorted population, but likely not enough to rescue any significant viral activity in patients. When comparing V1 to the E166V, Y154N double mutation variant, the addition of A285G increased resistance to nirmatrelvir somewhat, while overall catalytic efficiency increased almost 2-fold. It is worth noting that although the A285G mutation has only appeared in the GISAID database 37 times so far, the A285V mutation (not enriched in our sorted population) is showing up commonly in the most recent sequences in the database, having been deposited over 8000 times so far, and climbing.[36] This compares to the other two most common SARS-CoV-2 M^{pro} mutations, P132H and K90R, that have appeared just over 9 million times and over 220000 times, respectively.[36] Neither of these two latter mutations appeared as enriched in our sorted population.

Further analyses of the most highly enriched mutations in our sorted population found enrichment linkages that we refer to as V2−V4 in Table 1 as well as in Figures 3 and S4 . For V2, there was lower overall resistance to nirmatrelvir, but a 9-fold increase in catalytic activity with the substrate compared to its most resistant individual mutation that is once again E166V. The higher overall catalytic activity of V2 with the substrate is presumably why it was present as an enriched combination in our sorted population. It is worth noting that when analyzed alone, the H80L mutation identified as part of V2, displayed a higher catalytic efficiency (k_{cat}/K_M) with the AVLQ↓SGFR substrate (mostly due to a lower K_M) compared to that of the original SARS-CoV-2 M^{pro}. Both V3 and V4 displayed higher resistance to nirmatrelvir binding compared to their most resistant individual mutations, L27V and H64L, respectively. Despite being overall the least resistant of the enriched mutation combinations we studied, V3 displayed the highest catalytic efficiency with the AVLQ↓SGFR substrate compared to the other combination variants V1, V2, and V4. Although V3's higher overall catalytic activity with the substrate likely explains why it was enriched as a combination in our sorted population, the original SARS-CoV-2 M^{pro} is still 5-fold more active with the AVLQ↓SGFR substrate. By way of contrast, compared to V3, V4 displayed 40-fold higher resistance to nirmatrelvir but around 5-fold lower catalytic activity with the AVLQ↓SGFR substrate (still 30-fold lower activity compared to the original SARS-CoV-2 M^{pro}).

We analyzed three SARS-CoV-2 M^{pro} mutations, P132H, K90R, and A285 V, that are currently appearing commonly in viral isolates from patients with COVID-19. The P132H mutation displays a 3-fold compromised catalytic activity with the AVLQ↓SGFR substrate compared to the original SARS-CoV-2 M^{pro}. Our results alone do not provide a clear explanation for why the P132H mutation became common after appearing very early in the COVID-19 pandemic. On the other hand, the addition of the K90R mutation along with P132H restores catalytic efficiency to that seen for the original SARS-CoV-2 M^{pro}, likely revealing that selective pressure for restored catalytic efficiency was present as the pandemic continued. These two mutations appeared before nirmatrelvir was introduced, so it is not surprising that neither one alone nor the combination increases resistance.

The more recent surge of the A285V mutation in combination with both P132H and K90R has come after the introduction of nirmatrelvir as a frontline treatment for COVID-19. It is therefore reasonable to expect that A285V might provide resistance to nirmatrelvir. Our results indicate that this is true to some extent. The P132H, K90R, A285V triple mutation variant was indeed greater than 20-fold more resistant to nirmatrelvir compared to the original SARS-CoV-2 M^{pro} or the P132H, K90R double mutation variant. However, once again, just like we observed with the mutations isolated in our YESS 2.0 screens, the increased nirmatrelvir resistance seen with the P132H, K90R, A282V triple mutation variant comes at the expense of a 6-fold loss of catalytic efficiency with the AVLQ↓SGFR substrate. It is worth pointing out that crystallographic analysis confirms that P132H, K90R, and A285V are not located near the SARS-CoV-2 M^{pro} active site, so any influence on catalytic activity is likely to be indirect (see the violet side chains in Figure 5B). Interestingly, A285 is part of the SARS-CoV-2 M^{pro} dimer interface, as the A285 side chain methyl groups of each monomer are in contact with each other in the native dimer structure, possibly indicating that the details of dimerization are somehow related to the activity changes seen with the A285V variant.

Any change in SARS-CoV-2 M^{pro} protease specificity, even a subtle change, would likely require a compensatory change in the COVID-19 viral polyprotein cleavage sequences. This also likely explains why so few SARS-CoV-2 M^{pro} mutations have shown up in the GISAID data thus far in the pandemic. The

https://doi.org/10.1021/acsbiomedchemau.4c00045
ACS Bio Med Chem Au 2024, 4, 280−290

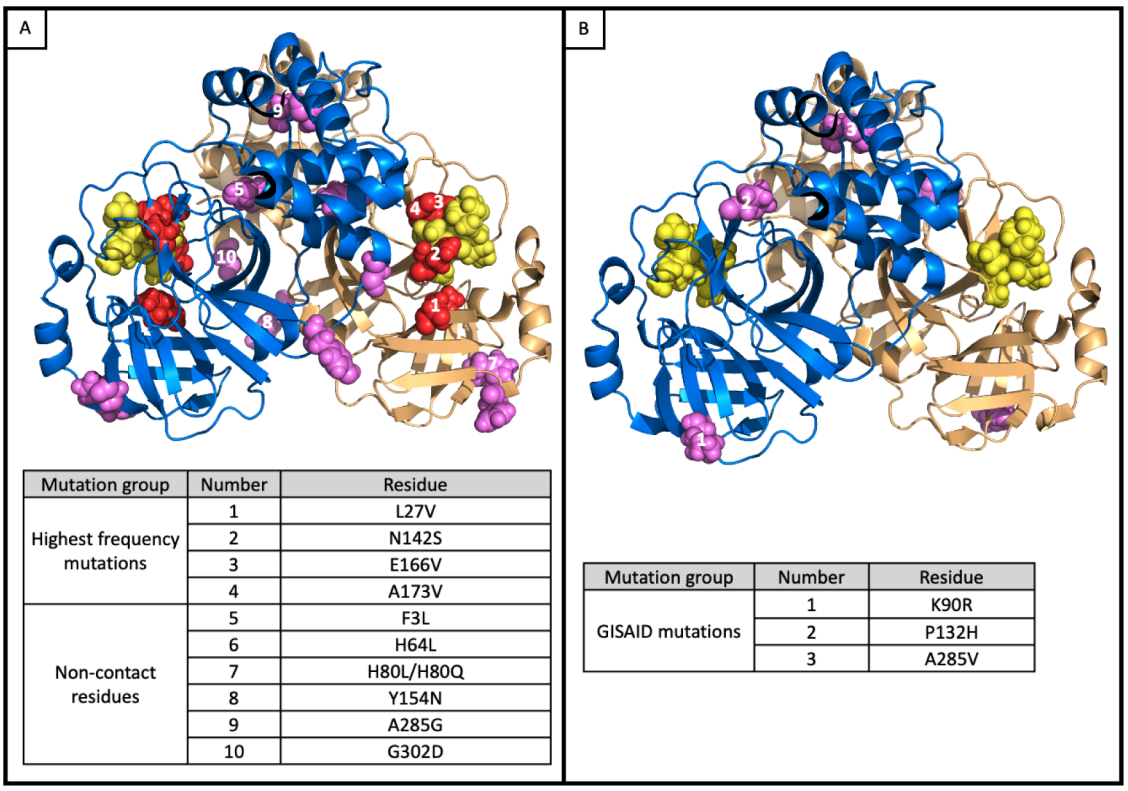

Mutation group	Number	Residue
Highest frequency mutations	1	L27V
	2	N142S
	3	E166V
	4	A173V
Non-contact residues	5	F3L
	6	H64L
	7	H80L/H80Q
	8	Y154N
	9	A285G
	10	G302D

Mutation group	Number	Residue
GISAID mutations	1	K90R
	2	P132H
	3	A285V

Figure 5. Locations of the highest frequency mutations and GISAID mutations in SARS CoV-2 M^{pro} (PDB entry 8B2T). Yellow spheres are bound nirmatrelvir. Blue (monomer chain 1) and light orange (monomer chain 2) are used to trace the backbones of the two SARS-CoV-2 M^{pro} monomers that combine to make a functional dimeric enzyme. (A) The highest frequency mutations identified in our SARS-CoV-2 M^{pro} resistance screen are shown in red spheres for residues that contact the inhibitor and violet for noncontact residues. (B) The three highest frequency SARS-CoV-2 M^{pro} mutations in the GISAID database.

present work adds to a growing list of mutations[14−35] that have been isolated *in vitro* and are known to decrease nirmatrelvir binding to SARS-CoV-2 M^{pro}. *In fact, the extremely high throughput nature of our screen has added 100 possible mutations to that list* (Table S1). Importantly, within the list of the most common mutations we found are the most prominent mutations identified using other methodologies, especially E166V, A173V, S144A, and H172Q.[14,15,18,20−22,24,26,30,33,34] Other reported mutations of note that we did not find in large numbers or at all from our screen include T21I, L50F, E166A, L176F, Q192R, and T304I[20,23,24,29,30,33] (Table S2). Possible explanations include the stochastic nature of the library construction process that cannot cover all of the sequence space as well as the different selection strategies that might favor different mutations. In particular, the YESS 2.0 system selects for resistance against a background of cleaving only a single preferred substrate, unlike screens based on viral replication that are likely to be sensitive to the various other polyprotein cleavage sequences needed to assemble a functional virus. It is worth emphasizing that of the 100 mutations we identified, *none* appear to have been increasing in the GISAID database after the introduction of Paxlovid as a front-line treatment (Table S1), although we note that E166A/V was reported after prolonged treatment with nirmatrelvir and other drugs in a highly immunocompromised COVID patient.[46]

The overall results with the most common mutations isolated using our YESS 2.0 system indicate that resistance to nirmatrelvir binding comes at the expense of lower catalytic efficiency with the substrate. *This was true for the most enriched individual mutation variants and the most enriched combination mutation variants we isolated in our YESS 2.0 screens, as well as the P132H, K90R, A282V triple mutation variant that is currently commonly appearing in the GISAID database.* A similar finding was reported for the L50F, E166A, and L176F individual mutations as well as the combination.[29,31] This trade-off should not come as a surprise, perhaps, because the nirmatrelvir structure can be viewed as a rigidified yet faithful mimic of the Val-Leu-Gln sequence for P3−P1, exactly the sequence we determined to be the most highly enriched in our SARS-CoV M^{pro} and SARS-CoV-2 M^{pro} substrate specificity profiling experiments[6] (see Figure 4). Because of this structural similarity, the majority of SARS-CoV-2 M^{pro} mutations, individually or in combinations, that disrupts binding to nirmatrelvir will therefore also be expected to compromise substrate recognition and cleavage.[40] We note that mimicking P1−P3 with an attached warhead is a common strategy in protease inhibitor design.[47,48] SARS-CoV-2 M^{pro} might be especially sensitive to even small alterations in substrate interactions because of the subtle recognition involved during cleavage of the 11 different sites in the polyprotein with different specific relative rates that are presumably finely tuned by evolution to facilitate efficient viral assembly. It is worth noting that a lack of emerging resistance to nirmatrelvir might also be due in part to the short treatment duration commonly used; only 5 days are recommended, perhaps limiting the opportunity for resistance to emerge in any one patient.

The optimistic conclusion from our work, as well as from monitoring emerging SARS-CoV-2 viral sequences,[2,13,24,27,28,34,35] is that Paxlovid could be a useful frontline treatment for COVID-19 significantly longer than might have been expected based on experience with other viral protease

https://doi.org/10.1021/acsbiomedchemau.4c00045
ACS Bio Med Chem Au 2024, 4, 280−290

inhibitors such as those used to treat HIV infections. Based on the remarkable similarity between the M^{pro} enzyme targets, the same should be true if nirmatrelvir or a close derivative is ever used to treat a future outbreak of SARS. Future work will reveal if the close structural correspondence between an inhibitor (such as nirmatrelvir) and its target's preferred substrate will indeed represent a powerful general strategy to limit the emergence of resistance during viral infections.

MATERIALS AND METHODS

Substrate Assembly (Aga2-His-Flag-AVLQSGFR-HA-ER), SARS-CoV-2 M^{pro} Gene Cloning into pYESS2, and SARS-CoV-2 M^{pro} Activity Screen Were Performed as Described[6]

Inhibition Screen in YESS 2.0. Clones were picked from the transformed pYESS2-SARS-CoV-2 M^{pro} substrate and incubated overnight in YNB-CAA-glucose liquid media at 30 °C. The saturated culture was reinoculated at an OD of 1 and incubated at 30 °C until an OD of 2−5 was reached. This was induced in a concentration range of nirmatrelvir (5−1000 μM)-YNB-CAA-galactose at 25 °C for 14−16 h and ±2 μM β-estradiol for positive and negative controls, respectively. The cells were washed in ice-cold PBS + 0.5% BSA and labeled in ice-cold PBS + 0.5% BSA with anti-FLAG-PE (BioLegend, 0.25 μL/10^7 cells) and anti-HA-FITC (GenScript, 0.5 μL/10^7 cells) antibodies at a concentration of 10^5 cells/μL and incubated on ice, in the dark, for 1 h. The cells were then washed in PBS + 0.5% BSA and screened by FACS BD Aria.

Library Sorting and Screen. The library was induced using YNB-CAA-galactose at 25 °C for 14−16 h in the presence of β-estradiol and nirmatrelvir for the first sort round and 10× the size of the library was labeled using anti-Flag-PE and anti-HA-FITC. The population displaying loss of HA-FITC fluorophore while maintaining FLAG-PE was sorted using FACS. The collected cells were added to an ample volume of YNB-CAA-glucose and recovered at 30 °C then reinoculated at an OD of 1 and induced at an OD of 2−5 using YNB-CAA-galactose at 25 °C for 14−16 h ± β-estradiol with increasing concentration of nirmatrelvir. The cells were then labeled with anti-Flag-PE and anti-HA-FITC, and the enriched population was sorted. Several rounds of sorting were needed to reach a 90−95% shift of the population for loss of the HA-FITC signal. This was followed by a screening process to confirm the population enrichment. After being sorted, the cells were plated on YNB-CAA-glucose plates, and individual colonies were sequenced and screened using FACS.

PacBio Analysis. The raw data for both the naïve and the sorted were filtered to remove any stop codon in the substrate cassette, and sequence enrichment was made by comparing the number of sequences in the naïve library and the sorted library. The heatmap and frequency table were generated. Residue, dimer, and combination enrichment were also determined. This bioinformatic analysis was performed by the Center for Biomedical Research Support at the University of Texas at Austin.

Expression and Purification of SARS-CoV2M^{pro}. As described in [49,50], SARS-CoV-2 M^{pro} the original and the variants fused to a 6xHis tag were cloned into pET21(+)b using NdeI and *Bam*HI sites. Then, they were transformed into *E. coli* BL21(DE)-pLysS (Thermofisher Scientific). Several colonies were grown in 2xYT-ampicillin/chloramphenicol media at 37 °C and induced in 1 mM IPTG for 16−20 h. The bacterial cultures were pelleted and lysed in lysis buffer (50 mM Tris, 0.5 M NaCl, 1 mM DTT, 20 mM imidazole, and 10% glycerol). The purification was carried out on a Ni-NTA column eluted with 250 mM imidazole, dialyzed, and stored in storage buffer (50 mM Tris, 0.1 M NaCl, 1 mM DTT, 10% glycerol). The purified enzyme was snap-frozen in liquid N_2 and stored at −80 °C.

***In Vitro* Inhibition Assay.** As described in 7, serial dilutions of nirmatrelvir were made with a final concentration range between 1 mM and 0.01 nM in the activity assay buffer (20 mM Tris-HCL, pH 7.3, 100 mM NaCl, 1 mM EDTA, 5 mM TCEP). The inhibitor was incubated with the enzyme for 20 min at 37 °C followed by the addition of 4 mM of the substrate (Abz-AVLQSGFR-Lys(Dnp)), and the reaction progress was monitored at Ex/Em of 320 nm/420 nm using an HT-Synergy plate reader at 30 °C. Reactions at each concentration were run in triplicate. The data was analyzed and fitted using GraphPad Prism software (version 9.1.2).

ASSOCIATED CONTENT

Supporting Information

The Supporting Information is available free of charge at https://pubs.acs.org/doi/10.1021/acsbiomedchemau.4c00045.

Nirmatrelvir inhibition of SARS-CoV-2 M^{pro}; SARS-CoV M^{pro} resistant mutation screen in YESS2.0; FACS screen of nirmatrelvir inhibition of single mutation variants of SARS-CoV-2 M^{pro}; top 100 mutations of SARS-CoV-2 M^{pro} in our PacBio data; previously reported mutations of SARS-CoV-2 M^{pro}; combination variants of SARS-CoV-2 M^{pro} location in SARS-CoV-2 M^{pro} structure; FACS screen for nirmatrelvir inhibition of combination mutation variants of SARS-CoV-2 M^{pro}; FACS screen for nirmatrelvir inhibition of double mutation variants of SARS-CoV-2 M^{pro}; FACS screen for nirmatrelvir inhibition of single and combination mutation variants of SARS-CoV-2 M^{pro} reported in GSAID database (PDF)

AUTHOR INFORMATION

Corresponding Author

Brent L. Iverson − *Department of Chemistry, The University of Texas at Austin, Austin, Texas 78712, The United States of America*; orcid.org/0000-0001-7974-3605; Email: iversonb@austin.utexas.edu

Authors

Rasha M. Yaghi − *Department of Chemistry, The University of Texas at Austin, Austin, Texas 78712, The United States of America*; orcid.org/0009-0006-8639-497X

Dennis C. Wylie − *Center of Biomedical Research Support, The University of Texas at Austin, Austin, Texas 78712, The United States of America*

Collin L. Andrews − *Department of Chemistry, The University of Texas at Austin, Austin, Texas 78712, The United States of America*

Olivia H. Dickert − *Department of Chemistry, The University of Texas at Austin, Austin, Texas 78712, The United States of America*

Anjana Ram − *Department of Chemistry, The University of Texas at Austin, Austin, Texas 78712, The United States of America*

Complete contact information is available at: https://pubs.acs.org/10.1021/acsbiomedchemau.4c00045

Author Contributions

R.M.Y. and B.L.I. designed the research, R.M.Y., A.R., and O.H.D. performed the research, R.M.Y., C.L.A., D.C.W., and B.L.I. analyzed the data, and R.M.Y. and B.L.I. wrote the manuscript. CRediT: **Rasha M. Yaghi** conceptualization, data curation, formal analysis, investigation, methodology, validation, visualization, writing-original draft, writing-review & editing; **Dennis C. Wylie** data curation, formal analysis, validation, visualization; **Collin L. Andrews** data curation, formal analysis, validation, visualization; **Olivia H Dickert** investigation; **Anjana Ram** investigation; **Brent L. Iverson** conceptualization, formal

https://doi.org/10.1021/acsbiomedchemau.4c00045
ACS Bio Med Chem Au 2024, 4, 280−290

analysis, funding acquisition, methodology, project administration, resources, supervision, visualization, writing-original draft, writing-review & editing.

Funding

This work was supported by the Clayton Foundation for Research (to B.L.I).

Notes

The authors declare no competing financial interest.

■ ACKNOWLEDGMENTS

We would like to acknowledge the Center for Biomedical Research Support at the University of Texas at Austin for help with computational analysis of our datasets. We would also like to thank Dr. Kenneth Johnson, Dr. Li Yi, Dr. Everett Stone, and Dr. George Georgiou for many helpful discussions.

■ ABBREVIATIONS

SARS	severe acute respiratory syndrome
SARS-CoV	severe acute respiratory syndrome coronavirus
SARS-CoV-2	severe acute respiratory syndrome coronavirus 2
FACS	fluorescence activated cell sorting
NGS	next-generation sequencing
YESS2.0	yeast endoplasmic reticulum sequestration screening 2.0

■ REFERENCES

(1) Hu, Q.; Xiong, Y.; Zhu, G.-H.; Zhang, Y.-N.; Zhang, Y.-W.; Huang, P.; Ge, G.-B. The SARS-CoV-2 Main Protease (M ^{pro}): Structure, Function, and Emerging Therapies for COVID-19. *MedComm* **2022**, *3* (3), No. e151.

(2) Parigger, L.; Krassnigg, A.; Schopper, T.; Singh, A.; Tappler, K.; Köchl, K.; Hetmann, M.; Gruber, K.; Steinkellner, G.; Gruber, C. C. Recent Changes in the Mutational Dynamics of the SARS-CoV-2 Main Protease Substantiate the Danger of Emerging Resistance to Antiviral Drugs. *Front. Med.* **2022**, *9*, 1061142.

(3) V'kovski, P.; Kratzel, A.; Steiner, S.; Stalder, H.; Thiel, V. Coronavirus Biology and Replication: Implications for SARS-CoV-2. *Nat. Rev. Microbiol.* **2021**, *19* (3), 155−170.

(4) Osipiuk, J.; Azizi, S.-A.; Dvorkin, S.; Endres, M.; Jedrzejczak, R.; Jones, K. A.; Kang, S.; Kathayat, R. S.; Kim, Y.; Lisnyak, V. G.; et al. Structure of Papain-like Protease from SARS-CoV-2 and Its Complexes with Non-Covalent Inhibitors. *Nat. Commun.* **2021**, *12* (1), 743.

(5) Zhang, L.; Lin, D.; Sun, X.; Curth, U.; Drosten, C.; Sauerhering, L.; Becker, S.; Rox, K.; Hilgenfeld, R. Crystal Structure of SARS-CoV-2 Main Protease Provides a Basis for Design of Improved α-Ketoamide Inhibitors. *Science* **2020**, *368* (6489), 409−412.

(6) Yaghi, R. M.; Andrews, C. L.; Wylie, D. C.; Iverson, B. L. High-Resolution Substrate Specificity Profiling of SARS-CoV-2 M ^{pro}; Comparison to SARS-CoV M ^{pro}. *ACS Chem. Biol.* **2024**, *19* (7), 1474−1483.

(7) Owen, D. R.; Allerton, C. M. N.; Anderson, A. S.; Aschenbrenner, L.; Avery, M.; Berritt, S.; Boras, B.; Cardin, R. D.; Carlo, A.; Coffman, K. J.; et al. An Oral SARS-CoV-2 M ^{pro} Inhibitor Clinical Candidate for the Treatment of COVID-19. *Science* **2021**, *374* (6575), 1586−1593.

(8) Halford, B. The Path to Paxlovid. *ACS Cent. Sci.* **2022**, *8* (4), 405−407.

(9) Joyce, R. P.; Hu, V. W.; Wang, J. The History, Mechanism, and Perspectives of Nirmatrelvir (PF-07321332): An Orally Bioavailable Main Protease Inhibitor Used in Combination with Ritonavir to Reduce COVID-19-Related Hospitalizations. *Med. Chem. Res.* **2022**, *31* (10), 1637−1646.

(10) Zhao, Y.; Fang, C.; Zhang, Q.; Zhang, R.; Zhao, X.; Duan, Y.; Wang, H.; Zhu, Y.; Feng, L.; Zhao, J.; et al. Crystal Structure of SARS-CoV-2 Main Protease in Complex with Protease Inhibitor PF-07321332. *Protein Cell* **2022**, *13* (9), 689−693.

(11) Shah, D.; Freas, C.; Weber, I. T.; Harrison, R. W. Evolution of Drug Resistance in HIV Protease. *BMC Bioinf.* **2020**, *21* (S18), 497.

(12) Weber, I. T.; Agniswamy, J. HIV-1 Protease: Structural Perspectives on Drug Resistance. *Viruses* **2009**, *1* (3), 1110−1136.

(13) Mótyán, J. A.; Mahdi, M.; Hoffka, G.; Tőzsér, J. Potential Resistance of SARS-CoV-2 Main Protease (Mpro) against Protease Inhibitors: Lessons Learned from HIV-1 Protease. *Int. J. Mol. Sci.* **2022**, *23* (7), 3507.

(14) Ou, J.; Lewandowski, E. M.; Hu, Y.; Lipinski, A. A.; Aljasser, A.; Colon-Ascanio, M.; Morgan, R. T.; Jacobs, L. M. C.; Zhang, X.; Bikowitz, M. J.; et al. A Yeast-Based System to Study SARS-CoV-2 Mpro Structure and to Identify Nirmatrelvir Resistant Mutations. *PloS Pathog.* **2023**, *19* (8), No. e1011592.

(15) Flynn, J. M.; Huang, Q. Y. J.; Zvornicanin, S. N.; Schneider-Nachum, G.; Shaqra, A. M.; Yilmaz, N. K.; Moquin, S. A.; Dovala, D.; Schiffer, C. A.; Bolon, D. N. A. Systematic Analyses of the Resistance Potential of Drugs Targeting SARS-CoV-2 Main Protease. *ACS Infect. Dis.* **2023**, *9* (7), 1372−1386.

(16) Flynn, J. M.; Samant, N.; Schneider-Nachum, G.; Barkan, D. T.; Yilmaz, N. K.; Schiffer, C. A.; Moquin, S. A.; Dovala, D.; Bolon, D. N. Comprehensive Fitness Landscape of SARS-CoV-2 Mpro Reveals Insights into Viral Resistance Mechanisms. *eLife* **2022**, *11*, No. e77433.

(17) Lee, J. T.; Yang, Q.; Gribenko, A.; Perrin, B. S.; Zhu, Y.; Cardin, R.; Liberator, P. A.; Anderson, A. S.; Hao, L. Genetic Surveillance of SARS-CoV-2 M ^{pro} Reveals High Sequence and Structural Conservation Prior to the Introduction of Protease Inhibitor Paxlovid. *mBio* **2022**, *13* (4), No. e00869−22.

(18) Padhi, A. K.; Tripathi, T. Hotspot Residues and Resistance Mutations in the Nirmatrelvir-Binding Site of SARS-CoV-2 Main Protease: Design, Identification, and Correlation with Globally Circulating Viral Genomes. *Biochem. Biophys. Res. Commun.* **2022**, *629*, 54−60.

(19) Sasi, V. M.; Ullrich, S.; Ton, J.; Fry, S. E.; Johansen-Leete, J.; Payne, R. J.; Nitsche, C.; Jackson, C. J. Predicting Antiviral Resistance Mutations in SARS-CoV-2 Main Protease with Computational and Experimental Screening. *Biochemistry* **2022**, *61* (22), 2495−2505.

(20) Iketani, S.; Mohri, H.; Culbertson, B.; Hong, S. J.; Duan, Y.; Luck, M. I.; Annavajhala, M. K.; Guo, Y.; Sheng, Z.; Uhlemann, A.-C.; et al. Multiple Pathways for SARS-CoV-2 Resistance to Nirmatrelvir. *Nature* **2023**, *613* (7944), 558−564.

(21) Chatterjee, S.; Bhattacharya, M.; Dhama, K.; Lee, S.-S.; Chakraborty, C. Resistance to Nirmatrelvir Due to Mutations in the Mpro in the Subvariants of SARS-CoV-2 Omicron: Another Concern? *Mol. Ther.-Nucleic Acids* **2023**, *32*, 263−266.

(22) Ip, J. D.; Chu, A. W.-H.; Chan, W.-M.; Leung, R. C.-Y.; Abdullah, S. M. U.; Sun, Y.; To, K. K.-W. Global Prevalence of SARS-CoV-2 3CL Protease Mutations Associated with Nirmatrelvir or Ensitrelvir Resistance. *eBiomedicine* **2023**, *91*, 104559.

(23) Heilmann, E.; Costacurta, F.; Moghadasi, S. A.; Ye, C.; Pavan, M.; Bassani, D.; Volland, A.; Ascher, C.; Weiss, A. K. H.; Bante, D.; et al. SARS-CoV-2 3CL ^{pro} Mutations Selected in a VSV-Based System Confer Resistance to Nirmatrelvir, Ensitrelvir, and GC376. *Sci. Transl. Med.* **2023**, *15* (678), No. eabq7360.

(24) Hu, Y.; Lewandowski, E. M.; Tan, H.; Zhang, X.; Morgan, R. T.; Zhang, X.; Jacobs, L. M. C.; Butler, S. G.; Gongora, M. V.; Choy, J.; et al. Naturally Occurring Mutations of SARS-CoV-2 Main Protease Confer Drug Resistance to Nirmatrelvir. *ACS Cent. Sci.* **2023**, *9* (8), 1658−1669.

(25) Jiang, H.; Zhou, Y.; Zou, X.; Hu, X.; Wang, J.; Zeng, P.; Li, W.; Zeng, X.; Zhang, J.; Li, J. Evaluation of the Inhibition Potency of Nirmatrelvir against Main Protease Mutants of SARS-CoV-2 Variants. *Biochemistry* **2023**, *62* (13), 2055−2064.

(26) Ramos-Guzmán, C. A.; Andjelkovic, M.; Zinovjev, K.; Ruiz-Pernía, J. J.; Tuñón, I. The Impact of SARS-CoV-2 3CL Protease Mutations on Nirmatrelvir Inhibitory Efficiency. Computational Insights into Potential Resistance Mechanisms. *Chem. Sci.* **2023**, *14* (10), 2686−2697.

https://doi.org/10.1021/acsbiomedchemau.4c00045
ACS Bio Med Chem Au 2024, 4, 280−290

(27) Ullrich, S.; Ekanayake, K. B.; Otting, G.; Nitsche, C. Main Protease Mutants of SARS-CoV-2 Variants Remain Susceptible to Nirmatrelvir. *Bioorg. Med. Chem. Lett.* **2022**, *62*, 128629.
(28) Sacco, M. D.; Hu, Y.; Gongora, M. V.; Meilleur, F.; Kemp, M. T.; Zhang, X.; Wang, J.; Chen, Y. The P132H Mutation in the Main Protease of Omicron SARS-CoV-2 Decreases Thermal Stability without Compromising Catalysis or Small-Molecule Drug Inhibition. *Cell Res.* **2022**, *32* (5), 498−500.
(29) Jochmans, D.; Liu, C.; Donckers, K.; Stoycheva, A.; Boland, S.; Stevens, S. K.; De Vita, C.; Vanmechelen, B.; Maes, P.; Trüeb, B.; et al. The Substitutions L50F, E166A, and L167F in SARS-CoV-2 3CLpro Are Selected by a Protease Inhibitor *In Vitro* and Confer Resistance To Nirmatrelvir. *mBio* **2023**, *14* (1), No. e02815−22.
(30) Duan, Y.; Zhou, H.; Liu, X.; Iketani, S.; Lin, M.; Zhang, X.; Bian, Q.; Wang, H.; Sun, H.; Hong, S. J.; et al. Molecular Mechanisms of SARS-CoV-2 Resistance to Nirmatrelvir. *Nature* **2023**, *622* (7982), 376−382.
(31) Kiso, M.; Furusawa, Y.; Uraki, R.; Imai, M.; Yamayoshi, S.; Kawaoka, Y. In Vitro and in Vivo Characterization of SARS-CoV-2 Strains Resistant to Nirmatrelvir. *Nat. Commun.* **2023**, *14* (1), 3952.
(32) Zhou, Y.; Gammeltoft, K. A.; Ryberg, L. A.; Pham, L. V.; Tjørnelund, H. D.; Binderup, A.; Hernandez, C. R. D.; Fernandez-Antunez, C.; Offersgaard, A.; Fahnøe, U.; et al. Nirmatrelvir-Resistant SARS-CoV-2 Variants with High Fitness in an Infectious Cell Culture System. *Sci. Adv.* **2022**, *8* (51), No. eadd7197.
(33) Moghadasi, S. A.; Biswas, R. G.; Harki, D. A.; Harris, R. S. Rapid Resistance Profiling of SARS-CoV-2 Protease Inhibitors. *Npj Antimicrob. Resist.* **2023**, *1* (1), 9.
(34) Zhu, Y.; Yurgelonis, I.; Noell, S.; Yang, Q.; Guan, S.; Li, Z.; Hao, L.; Rothan, H.; Rai, D. K.; McMonagle, P.; Baniecki, M. L.; et al. In Vitro Selection and Analysis of SARS-CoV-2 Nirmatrelvir Resistance Mutations Contributing to Clinical Virus Resistance Surveillance. *Sci. Adv.* **2024**, *10* (30), No. eadl4013.
(35) Impact of SARS-CoV-2 Main Protease Mutations on Nirmatrelvir/Ritonavir (Paxlovid) Resistance; *Public Health Ontario*, https://www.publichealthontario.ca/-/media/Documents/nCoV/ipac/2022/06/sars-cov2-protease-mutations-paxlovid-resistance.pdf?sc_lang=en. accessed July 2022.
(36) Shu, Y.; McCauley, J. GISAID: Global initiative on sharing all influenza data − from vision to reality. *Eurosurveillance* **2017**, *22* (13), 30494.
(37) Denard, C. A.; Paresi, C.; Yaghi, R.; McGinnis, N.; Bennett, Z.; Yi, L.; Georgiou, G.; Iverson, B. L. YESS 2.0, a Tunable Platform for Enzyme Evolution, Yields Highly Active TEV Protease Variants. *ACS Synth. Biol.* **2021**, *10* (1), 63−71.
(38) Rhoads, A.; Au, K. F. PacBio Sequencing and Its Applications. *Genomics, Proteomics Bioinf.* **2015**, *13* (5), 278−289.
(39) Li, Q.; Yi, L.; Hoi, K. H.; Marek, P.; Georgiou, G.; Iverson, B. L. Profiling Protease Specificity: Combining Yeast ER Sequestration Screening (YESS) with Next Generation Sequencing. *ACS Chem. Biol.* **2017**, *12* (2), 510−518.
(40) McKimm-Breschkin, J. L.; Barrett, S.; McKenzie-Kludas, C.; McAuley, J.; Streltsov, V. A.; Withers, S. G. Passaging of an Influenza A(H1N1)Pdm09 Virus in a Difluoro Sialic Acid Inhibitor Selects for a Novel, but Unfit I106M Neuraminidase Mutant. *Antiviral Res.* **2019**, *169*, 104542.
(41) Johnson, K. A. *Kinetic Analysis for the New Enzymology: using Computer Simulation to Learn Kinetics and Solve Mechanisms*, 1st. Eds.; KinTek Corporation: Austin, TX, 2019.
(42) Shu, Y.; McCauley, J. GISAID: Global Initiative on Sharing All Influenza Data − from Vision to Reality. *Eurosurveillance* **2017**, *22* (13), 30494.
(43) Narwal, M.; Armache, J.-P.; Edwards, T. J.; Murakami, K. S. SARS-CoV-2 Polyprotein Substrate Regulates the Stepwise Mpro Cleavage Reaction. *J. Biol. Chem.* **2023**, *299* (5), 104697.
(44) Lee, J.; Kenward, C.; Worrall, L. J.; Vuckovic, M.; Gentile, F.; Ton, A.-T.; Ng, M.; Cherkasov, A.; Strynadka, N. C. J.; Paetzel, M. X-Ray Crystallographic Characterization of the SARS-CoV-2 Main Protease Polyprotein Cleavage Sites Essential for Viral Processing and Maturation. *Nat. Commun.* **2022**, *13* (1), 5196.
(45) Paciaroni, A.; Libera, V.; Ripanti, F.; Orecchini, A.; Petrillo, C.; Francisci, D.; Schiaroli, E.; Sabbatini, S.; Gidari, A.; Bianconi, E.; et al. Stabilization of the Dimeric State of SARS-CoV-2 Main Protease by GC376 and Nirmatrelvir. *Int. J. Mol. Sci.* **2023**, *24* (7), 6062.
(46) Hirotsu, Y.; Kobayashi, H.; Kakizaki, Y.; Saito, A.; Tsutsui, T.; Kawaguchi, M.; Shimamura, S.; Hata, K.; Hanawa, S.; Toyama, J.; et al. Multidrug-Resistant Mutations to Antiviral and Antibody Therapy in an Immunocompromised Patient Infected with SARS-CoV-2. *Med* **2023**, *4* (11), 813−824.e4.
(47) Hu, X.; Compton, J. R.; Leary, D. H.; Olson, M. A.; Lee, M. S.; Cheung, J.; Ye, W.; Ferrer, M.; Southall, N.; Jadhav, A.; et al. Mutational, and Structural Studies of the Venezuelan Equine Encephalitis Virus Nonstructural Protein 2 Cysteine Protease. *Biochemistry* **2016**, *55* (21), 3007−3019.
(48) Müller, P.; Meta, M.; Meidner, J. L.; Schwickert, M.; Meyr, J.; Schwickert, K.; Kersten, C.; Zimmer, C.; Hammerschmidt, S. J.; Frey, A. Investigation of the Compatibility between Warheads and Peptidomimetic Sequences of Protease Inhibitors—A Comprehensive Reactivity and Selectivity Study. *Int. J. Mol. Sci.* **2023**, *24* (8), 7226.
(49) Pablos, I.; Machado, Y.; De Jesus, H. C. R.; Mohamud, Y.; Kappelhoff, R.; Lindskog, C.; Vlok, M.; Bell, P. A.; Butler, G. S.; Grin, P. M.; et al. Mechanistic Insights into COVID-19 by Global Analysis of the SARS-CoV-2 3CLpro Substrate Degradome. *Cell Rep.* **2021**, *37* (4), 109892.
(50) Razali, R.; Subbiah, V. K.; Budiman, C. Technical Data of Heterologous Expression and Purification of SARS-CoV-2 Proteases Using *Escherichia Coli* System. *Data* **2021**, *6* (9), 99.

https://doi.org/10.1021/acsbiomedchemau.4c00045
ACS Bio Med Chem Au 2024, 4, 280−290